This is an open access article published under an ACS AuthorChoice License, which permits copying and redistribution of the article or any adaptations for non-commercial purposes.

ACS MATERIALS LETTERS

Cite This: ACS Materials Lett. 2019, 1, 272–276

www.acsmaterialslett.org

LETTER

Wide-Angle X-ray Diffraction Evidence of Structural Coherence in $CsPbBr_3$ Nanocrystal Superlattices

Stefano Toso,[†] Dmitry Baranov,*[,†] Cinzia Giannini,*[,‡] Sergio Marras,[†] and Liberato Manna*[,†]

[†]Nanochemistry Department, Istituto Italiano di Tecnologia, Via Morego 30, 16163 Genova, Italy

[‡]Istituto di Cristallografia - Consiglio Nazionale delle Ricerche (IC-CNR), via Amendola 122/O, I-70126 Bari, Italy

Supporting Information

ABSTRACT: **Films made of colloidal $CsPbBr_3$ nanocrystals packed in isolated or densely-packed superlattices display a remarkably high degree of structural coherence. The structural coherence is revealed by the presence of satellite peaks accompanying Bragg reflections in wide-angle X-ray diffraction experiments in parallel-beam reflection geometry. The satellite peaks, also called "superlattice reflections", arise from the interference of X-rays diffracted by the atomic planes of the orthorhombic perovskite lattice. The interference is due to the precise spatial periodicity of the nanocrystals separated by organic ligands in the superlattice. The presence of satellite peaks is a fingerprint of the high crystallinity and long-range order of nanocrystals, comparable to those of multilayer superlattices prepared by physical methods. The angular separation between satellite peaks is highly sensitive to changes in the superlattice periodicity. These characteristics of the satellite peaks are exploited to track the superlattice compression under vacuum, as well as to observe the superlattice growth in situ from colloidal solutions by slow solvent evaporation.**

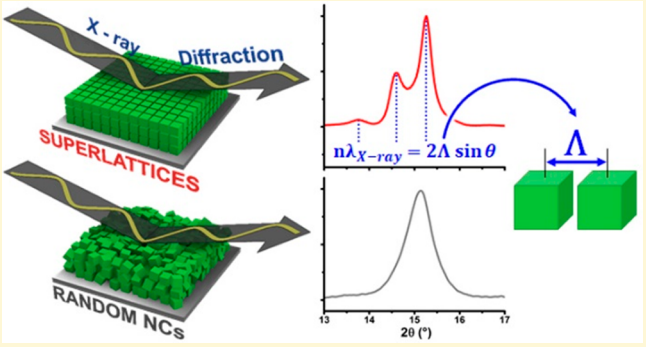

Since 2015,[1] colloidal nanocrystals (NCs) of lead halide perovskites (LHPs) have emerged as a class of promising nanomaterials for solution-processed light emitters and photovoltaics.[2−4] Thin films of randomly-oriented NCs and ordered NC arrays or superlattices (SLs) are forms of solid-state LHP materials alternative to polycrystalline films or single crystals of solution-processed bulk LHPs. Arranging NCs into SLs may reveal novel phenomena arising from the collective behavior of LHP NCs, as has been demonstrated by several studies of light-emission properties of $CsPbBr_3$ NC SLs.[5−8]

In this work, we investigate another collective phenomenon, namely, the structural coherence in three-dimensional SLs of $CsPbBr_3$ NCs grown on a flat silicon substrate. By structural coherence, we mean the combination of high crystallinity and long-range order of NCs in an SL to an extent comparable with the structural quality of multilayer SLs of metals or semiconductors prepared using molecular beam epitaxy,[9] sputtering,[10] or electrodeposition.[11] $CsPbBr_3$ NC SLs prepared by slow solvent evaporation show not only preferential alignment (commonly observed in arrays of orientationally ordered NCs)[12] but also "superlattice reflections"[9,13] in wide-angle X-ray diffraction (XRD) experiments (Figures 1a and 2)—the signature of structural coherence. The SL reflections appear as periodically spaced satellite peaks in the region of the Bragg reflections from (110), (1$\bar{1}$0), and (002) planes at $2\theta \sim 15°$ (Figure 2) and (220), (2$\bar{2}$0), and (004) planes at $2\theta \sim 30.5°$ (Figure S1) of the orthorhombic unit cell of $CsPbBr_3$ NCs. These satellite peaks are high-order Bragg reflections of the SL[10,13] generated by the interference of the reflections from the atomic planes of orthorhombic $CsPbBr_3$ NCs. The structural coherence arises from the combination of two features: (i) the high crystallinity, well-defined, and nearly identical shapes of the individual NCs and (ii) the regular NC packing, with little variation in the inter-NC spacing over large areas in the direction normal to the plane of the sample. Interestingly, this effect appears to be recurrent, as SL reflections of varying intensities can be identified by examination of the asymmetric or split shape of the $2\theta \sim 15°$ peak in the previously published XRD patterns,[14−19] but their origin remained unexplained.

The application of the Bragg law to the analysis of the satellite peaks[10] allowed us to extract the SL wavelength, Λ, from a single X-ray measurement in parallel-beam reflection θ/

Received: June 13, 2019
Accepted: July 16, 2019
Published: July 16, 2019

Downloaded via Dmitry Baranov on September 11, 2020 at 06:55:57 (UTC).
See https://pubs.acs.org/sharingguidelines for options on how to legitimately share published articles.

© 2019 American Chemical Society

DOI: 10.1021/acsmaterialslett.9b00217
ACS Materials Lett. 2019, 1, 272–276

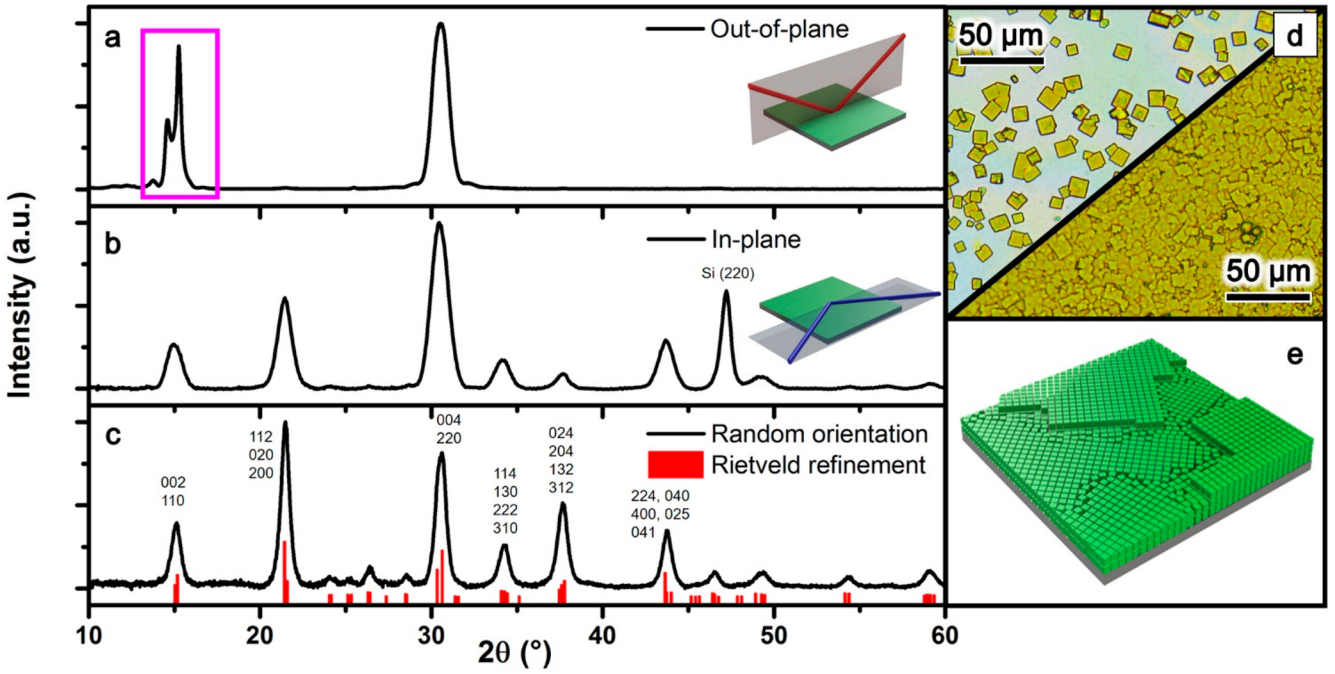

Figure 1. XRD patterns of (a) a film of densely packed $CsPbBr_3$ NC SLs measured in the out-of-plane reflection geometry. The splitting of the $2\theta \sim 15°$ peak (highlighted by the magenta box) is due to the SL effect. (b) The same sample measured in the in-plane geometry (a relatively sharp reflection at ~47.2° is assigned to the silicon substrate[20]). (c) Randomly oriented NCs mixed with amorphous silica (the reference pattern is based on the lattice parameters from Rietveld refinement: a = 8.2248 Å, b = 8.2741 Å, c = 11.7748 Å; Miller indices are provided for the six most intense reflections). (d) Optical microscopy images of the isolated SLs and a film of densely packed SLs of $CsPbBr_3$ NCs. Note that the peak splitting is observed in both types of samples (Figure S3). (e) Sketch of the film of densely-packed $CsPbBr_3$ NC SLs featuring domains with a coherent structure.

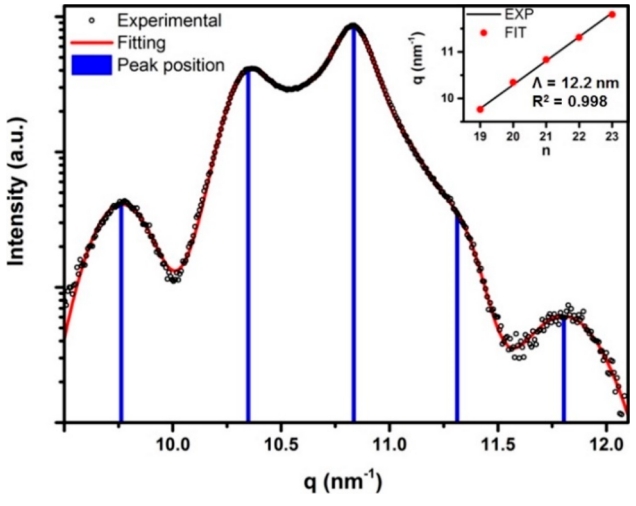

Figure 2. Closer look at the peak profile at $2\theta \sim 15°$. A section of the out-of-plane XRD data shown in Figure 1a was replotted on a logarithmic intensity scale vs scattering vector [q (nm^{-1})]. The circles are experimental data, and the continuous red line is a fit. The vertical drop lines indicate the position of the five satellite peaks originating from the SL. The inset shows the best linear fit of the centers of satellite peaks in q vs n, starting from n = 19 (corresponding to the SL wavelength, $\Lambda \sim 12.2$ nm).

2θ geometry. The utility of this parameter is demonstrated for two case studies: the contraction of NC SLs, hence the contraction of Λ, when the sample is put under vacuum (Figure 3), and the actual formation of the SLs upon slow solvent evaporation (Figure 4). Having a precise estimate of Λ that is independent of electron microscopy measurements is of key relevance for the study of LHP NC arrays, as NC orientation and spacing may strongly affect inter-NC effects, for example, exciton coupling.[21,22]

The samples of $CsPbBr_3$ NCs used in this work were synthesized following the hot-injection method[1] with optimized amounts of oleic acid and oleylamine,[17] as detailed in the prior work.[8] The NC SLs were grown on top of 1 × 1 cm Si substrates from tetrachloroethylene solutions by letting the solvent evaporate over several hours (see Materials and Methods section in Supporting Information (SI)). The XRD pattern of the resulting film measured in the out-of-plane $\theta/2\theta$ geometry is shown in Figure 1a. Two effects are immediately noticeable: a strong preferential alignment of NCs in the sample, manifested by the presence of two strong peaks at $2\theta \sim 15°$ and $2\theta \sim 30.5°$, and the splitting of the $2\theta \sim 15°$ peak into narrow peaks. A similar but much weaker splitting is observed for the peak at $2\theta \sim 30.5°$ (Figure S1). The XRD of the same sample measured in-plane (Figure 1b) or of NCs mixed with amorphous silica (Figure 1c) contained the Bragg reflections expected from orthorhombic $CsPbBr_3$.[14,23] The Rietveld refinement of the XRD pattern from randomly-oriented NCs yielded lattice parameters similar to one of the reference structures of orthorhombic $CsPbBr_3$ (ICSD No. 98-009-7851,[24] Figure S2 and Tables S1 and S3). The effect of peak splitting is reproducible and has been observed on the SL samples prepared from at least five different batches of $CsPbBr_3$ NCs.

The preferential alignment originates from the close-packing of the cubes in the plane parallel to the substrate and leads to the enhanced Bragg reflections from (110), (1$\bar{1}$0), and (002) ($2\theta \sim 15°$) and (220), (2$\bar{2}$0), and (004) ($2\theta \sim 30.5°$) planes of the orthorhombic unit cell of $CsPbBr_3$. The splitting of the

DOI: 10.1021/acsmaterialslett.9b00217
ACS Materials Lett. 2019, 1, 272−276

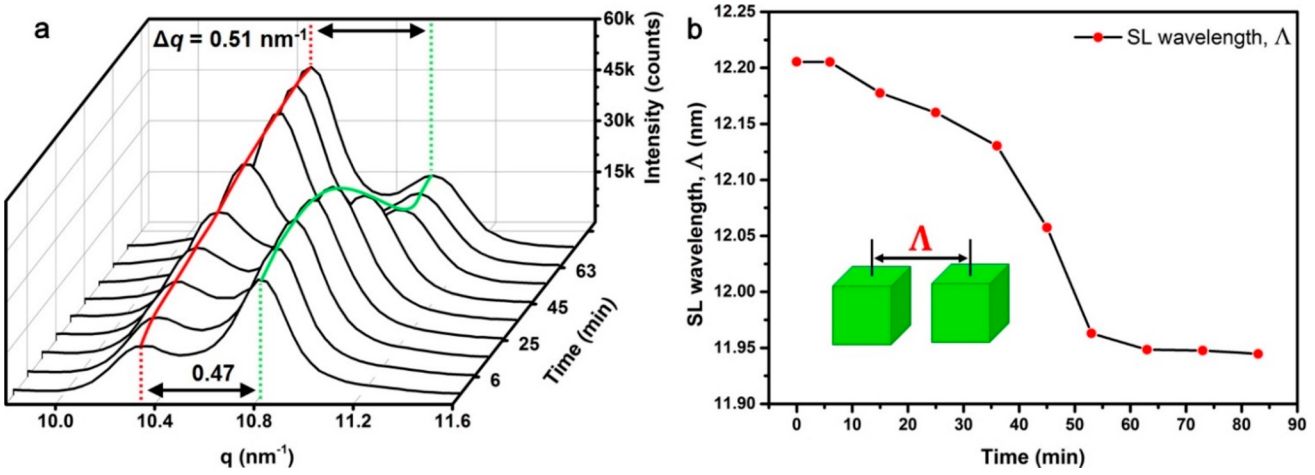

Figure 3. (a) Time evolution of the satellite peaks in the $2\theta \sim 15°$ region ($q \sim 10.6$ nm^{-1}) in the XRD pattern of the film of densely packed $CsPbBr_3$ NC SLs under static vacuum. (b) Corresponding contraction of the SL wavelength, Λ, as a function of time (red circles).

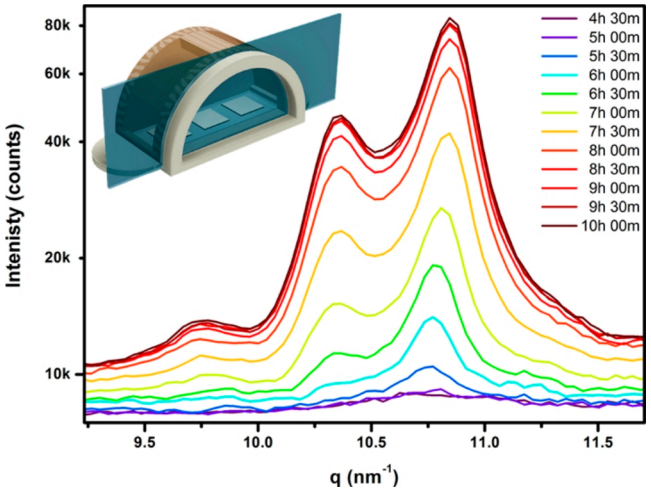

Figure 4. Emergence of the satellite peaks in the $2\theta \sim 15°$ region during the growth of a film of densely-packed $CsPbBr_3$ NC SLs from tetrachloroethylene solution. The figure reports a series of XRD patterns collected over 10 h at 30 min intervals. The inset is a sketch of the actually 3D-printed solvent evaporation chamber sealed with X-ray transparent Kapton and equipped with a sliding window on the side (blue-grey rectangle) to allow the placement of the sample.

peaks, most intense at the $2\theta \sim 15°$ and much weaker at $2\theta \sim 30.5°$, arises from the SL effect—an interference of X-rays diffracted by the atomic planes of the orthorhombic perovskite lattice due to the precise spatial periodicity of the NCs in the SL (see discussion of the physical origin below). The SL effect at wide angles in X-ray diffraction is observed in NC films of isolated or densely packed SLs (Figure 1d; see Figure S3 for the XRD pattern of the sample of isolated SLs). The comparison of optical and scanning electron microscopy images of isolated SLs and the films suggests that films consist of densely packed SLs and continuously cover the substrate except in areas next to the sample edges (Figures 1d and e and S4–S7).

A deeper inspection of the out-of-plane XRD pattern unraveled a fine structure for the $2\theta \sim 15°$ peak, better represented on a logarithmic intensity versus scattering vector scale (Figure 2). The conversion from the scattering angle, θ (in radians), to the scattering vector, q (in nm^{-1}), was done through the formula $q = (4\pi/\lambda_{X\text{-ray}}) \sin\theta$, where $\lambda_{X\text{-ray}} = 0.15406$ nm. The peak profile is composed of several contributions, which were fit to the total of six peaks described by Gaussian profiles on top of the background approximated by a 2nd order polynomial (Figure S8 and Table S2). Five out of six fitted peaks were assigned to the SL reflections, and one, with $q = 10.72$ nm^{-1} ($2\theta \sim 15.1°$), was ascribed to the atomic Bragg reflection of the $CsPbBr_3$ NCs on the basis that its position coincides with a corresponding peak from the XRD pattern of randomly oriented NCs.

The SL wavelength, Λ, order of satellite (n), and the corresponding peak center, q_n, are related by the formula $q_n = 2\pi n/\Lambda$, derived by rearranging the original expression for the orders of SL reflections: $\sin\theta_n = \frac{1}{2} n\Lambda/\lambda_{X\text{-ray}}$[10] (the expression is reproduced here with different notation). According to the best fit, $q_n = 0.51483n$ ($R^2 = 0.998$, Figure 2, inset) and $\Lambda \sim 12.2$ nm, and the first resolved satellite peak (at $q = 9.76$ nm^{-1}) corresponds to $n = 19$. However, n values 18 and 20 ($\Lambda \sim 11.6$ and 12.8 nm, respectively) also yielded a reasonable linear fit. Unequivocal discrimination between the different values of n is hindered by the broadening of the peaks. The best fit of SL wavelength $\Lambda \sim 12.2$ nm is comparable to ~11.6–12.5 nm for the period extracted from the fast Fourier transforms of the transmission electron microscopy images of close-packed $CsPbBr_3$ NCs (Figures S9–S11). The value of Λ is interpreted as an average center-to-center distance between the inorganic $CsPbBr_3$ cores inside the SL. The fitting of the XRD pattern in the region of $2\theta \sim 15°$ is meant to provide an accurate identification of the SL satellites for determination of the most likely value of Λ and is not a quantitative model of the observed effect.

The physical origins of the satellite peaks in XRD of thin film SLs and epitaxial quantum dots are well-documented in the literature.[13,25–27] For a qualitative explanation of the SL satellites observed in this work, let us consider the SL of $CsPbBr_3$ NCs as a periodic 3D array of X-ray scatterers separated by the period Λ. $CsPbBr_3$ NCs in the SL are crystalline particles which diffract X-rays in specific directions as determined by their crystal structure. The X-rays first diffracted by the atomic planes of the NCs undergo interference because of the phase shift caused by the periodicity of the SL. The diffraction from such a periodic array follows Bragg's law, producing reflections at $q_n = 2\pi n/\Lambda$:

DOI: 10.1021/acsmaterialslett.9b00217
ACS Materials Lett. 2019, 1, 272–276

the consequent constructive interference of diffracted X-rays leads to a series of closely and equally spaced reflections ($q_{n+1} - q_n = 2\pi/\Lambda$). Consequently, the satellite peaks appear only in the q range where there is diffraction by the atomic planes, and the intensities of the satellite peaks in the resulting diffraction pattern are modulated by the intensity profile of the NC diffraction peak.

An immediate utility of the satellite peaks for the characterization of $CsPbBr_3$ NC SLs comes from the recognition that the spacing between the peaks is inversely proportional to the SL wavelength, $\Delta q_n \propto 1/\Lambda$, and that spacing can be accessed through a straightforward X-ray diffraction measurement in a parallel-beam out-of-plane geometry. For example, a series of XRD patterns recorded on the $CsPbBr_3$ NC SLs placed under medium vacuum ($\sim 10^{-2}$ mbar) for ~70 min revealed a continuous change in the intensity, angular position, and separation of the satellite peaks in the $2\theta \sim 15°$ region, as shown in Figure 3a. The fitting of the satellite peaks following the procedure described above results in a progressively shrinking Λ (Figure 3b) from ~12.21 to ~11.95 nm (the number of figures after the decimal point reflects the average value of Λ). The SL contraction is irreversible, and the XRD pattern remains unchanged after the sample has been returned to atmospheric pressure (Figure S12). The contraction of Λ under vacuum has been reproduced on two different samples (Figures S13 and S14). Notably, the magnitude of a Λ contraction of ~0.25 nm (Figure 3b) is comparable to the length of the tetrachloroethylene molecule (~0.32 nm, calculated from the equilibrium distances and angles of C_2Cl_4),[28] suggesting the solvent removal as the main reason for a Λ contraction and explaining its irreversibility upon return to ambient pressure.

The presence of the satellite peaks is characteristic of the structural coherence in the material. Tracking the emergence of the satellite peaks with X-ray diffraction in situ during the formation of SLs is a non-invasive way of monitoring the growth process.[29] Figure 4 shows the appearance of the satellite peaks during tetrachloroethylene evaporation from the $CsPbBr_3$ NC solution deposited on top of the Si wafers (a replica of the process used for the preparation of the films described in this study, see Materials and Methods in SI). The process of tetrachloroethylene evaporation to dryness under ambient conditions takes ~10 h; however, the satellite peaks begin to emerge after ~6 h from the start of the experiment (cyan curve in Figure 4) and practically stop evolving after the total of ~8 h have passed, possibly indicating the completion of the SL formation process. Interestingly, the angular positions of the satellite peaks do not shift throughout the process of growth (the apparent shift of the peak at $2\theta \sim 15.2°$ during the ~4–6.5 h period is due to the transition from NCs suspended in the liquid to the SL structure), suggesting the retaining of the nearly constant Λ (~12.1 nm from the fitting) during the film growth.

In conclusion, the observation and analysis of the satellite peaks at wide angles in the X-ray diffraction of $CsPbBr_3$ NC SLs is presented. The structural coherence in the $CsPbBr_3$ NC SLs arises from the combination of high crystallinity, well-defined and nearly identical shapes of individual NCs, and regular packing with little variation in the inter-NC spacing over a large area. The fitting of the satellite peaks enables the determination of the SL wavelength, Λ, and its modulation under external conditions (e.g., contraction under vacuum). It is also shown how the emergence of the satellite peaks can be used to monitor the formation of the NC SLs in situ during the solvent evaporation. Remarkably, the presence of satellite peaks makes all these insights into the structure of $CsPbBr_3$ NC SLs accessible with a common X-ray diffraction setup.

■ ASSOCIATED CONTENT

Supporting Information

The Supporting Information is available free of charge on the ACS Publications website at DOI: 10.1021/acsmaterialslett.9b00217.

Materials and methods, XRD patterns of the samples of densely packed and isolated SLs, Rietveld refinement for randomly oriented NCs, fitting parameters for the satellite peaks, optical and scanning electron microscopy images of SLs, transmission electron microscopy images of $CsPbBr_3$ NCs, and additional XRD patterns for SL samples before and after application of vacuum (PDF)

■ AUTHOR INFORMATION

Corresponding Authors

*E-mail: dmitry.baranov@iit.it.
*E-mail: cinzia.giannini@ic.cnr.it.
*E-mail: liberato.manna@iit.it.

ORCID

Dmitry Baranov: 0000-0001-6439-8132
Cinzia Giannini: 0000-0003-0983-2885
Liberato Manna: 0000-0003-4386-7985

Author Contributions

The manuscript was written through contributions of all authors. All authors have given approval to the final version of the manuscript.

Notes

The authors declare no competing financial interest.

■ ACKNOWLEDGMENTS

The work of S.T. and L.M. was supported by the European Union under grant agreement no. 614897 (ERC Grant TRANS-NANO). The work of D.B. was supported by the European Union's Horizon 2020 research and innovation programme under the Marie Sklodowska-Curie grant agreement no. 794560 (RETAIN).

■ ABBREVIATIONS

XRD, X-ray diffraction; NC, nanocrystal; SL, superlattice

■ REFERENCES

(1) Protesescu, L.; Yakunin, S.; Bodnarchuk, M. I.; Krieg, F.; Caputo, R.; Hendon, C. H.; Yang, R. X.; Walsh, A.; Kovalenko, M. V. Nanocrystals of Cesium Lead Halide Perovskites ($CsPbX_3$, X = Cl, Br, and I): Novel Optoelectronic Materials Showing Bright Emission with Wide Color Gamut. *Nano Lett.* **2015**, *15*, 3692–3696.

(2) Kovalenko, M. V.; Protesescu, L.; Bodnarchuk, M. I. Properties and potential optoelectronic applications of lead halide perovskite nanocrystals. *Science* **2017**, *358*, 745–750.

(3) Akkerman, Q. A.; Rainò, G.; Kovalenko, M. V.; Manna, L. Genesis, challenges and opportunities for colloidal lead halide perovskite nanocrystals. *Nat. Mater.* **2018**, *17*, 394–405.

(4) Shamsi, J.; Urban, A. S.; Imran, M.; De Trizio, L.; Manna, L. Metal Halide Perovskite Nanocrystals: Synthesis, Post-Synthesis Modifications, and Their Optical Properties. *Chem. Rev.* **2019**, *119*, 3296–3348.

DOI: 10.1021/acsmaterialslett.9b00217
ACS Materials Lett. 2019, 1, 272–276

(5) Jurow, M. J.; Lampe, T.; Penzo, E.; Kang, J.; Koc, M. A.; Zechel, T.; Nett, Z.; Brady, M.; Wang, L.-W.; Alivisatos, A. P.; Cabrini, S.; Brütting, W.; Liu, Y. Tunable Anisotropic Photon Emission from Self-Organized $CsPbBr_3$ Perovskite Nanocrystals. *Nano Lett.* **2017**, *17*, 4534−4540.
(6) Rainò, G.; Becker, M. A.; Bodnarchuk, M. I.; Mahrt, R. F.; Kovalenko, M. V.; Stöferle, T. Superfluorescence from Lead Halide Perovskite Quantum Dot Superlattices. *Nature* **2018**, *563*, 671−675.
(7) Tong, Y.; Yao, E.-P.; Manzi, A.; Bladt, E.; Wang, K.; Döblinger, M.; Bals, S.; Müller-Buschbaum, P.; Urban, A. S.; Polavarapu, L.; Feldmann, J. Spontaneous Self-Assembly of Perovskite Nanocrystals into Electronically Coupled Supercrystals: Toward Filling the Green Gap. *Adv. Mater.* **2018**, *30*, 1801117.
(8) Baranov, D.; Toso, S.; Imran, M.; Manna, L. Investigation into the Photoluminescence Red Shift in Cesium Lead Bromide Nanocrystal Superlattices. *J. Phys. Chem. Lett.* **2019**, *10*, 655−660.
(9) Segmuller, A.; Krishna, P.; Esaki, L. X-ray diffraction study of a one-dimensional GaAs-AlAs superlattice. *J. Appl. Crystallogr.* **1977**, *10*, 1−6.
(10) Schuller, I. K. New Class of Layered Materials. *Phys. Rev. Lett.* **1980**, *44*, 1597−1600.
(11) Lashmore, D. S.; Dariel, M. P. Electrodeposited Cu-Ni Textured Superlattices. *J. Electrochem. Soc.* **1988**, *135*, 1218−1221.
(12) Murray, C. B.; Kagan, C. R.; Bawendi, M. G. Self-Organization of CdSe Nanocrystallites into Three-Dimensional Quantum Dot Superlattices. *Science* **1995**, *270*, 1335−1338.
(13) Holý, V. C.; Pietsch, U.; Baumbach, T. *High-Resolution X-ray Scattering from Thin Films and Multilayers*; Springer: Berlin, 1999; p xi, 256 p.
(14) Bertolotti, F.; Protesescu, L.; Kovalenko, M. V.; Yakunin, S.; Cervellino, A.; Billinge, S. J. L.; Terban, M. W.; Pedersen, J. S.; Masciocchi, N.; Guagliardi, A. Coherent Nanotwins and Dynamic Disorder in Cesium Lead Halide Perovskite Nanocrystals. *ACS Nano* **2017**, *11*, 3819−3831.
(15) Lorenzon, M.; Sortino, L.; Akkerman, Q.; Accornero, S.; Pedrini, J.; Prato, M.; Pinchetti, V.; Meinardi, F.; Manna, L.; Brovelli, S. Role of Nonradiative Defects and Environmental Oxygen on Exciton Recombination Processes in $CsPbBr_3$ Perovskite Nanocrystals. *Nano Lett.* **2017**, *17*, 3844−3853.
(16) Palazon, F.; Almeida, G.; Akkerman, Q. A.; De Trizio, L.; Dang, Z.; Prato, M.; Manna, L. Changing the Dimensionality of Cesium Lead Bromide Nanocrystals by Reversible Postsynthesis Transformations with Amines. *Chem. Mater.* **2017**, *29*, 4167−4171.
(17) Almeida, G.; Goldoni, L.; Akkerman, Q.; Dang, Z.; Khan, A. H.; Marras, S.; Moreels, I.; Manna, L. Role of Acid−Base Equilibria in the Size, Shape, and Phase Control of Cesium Lead Bromide Nanocrystals. *ACS Nano* **2018**, *12*, 1704−1711.
(18) Dutta, A.; Dutta, S. K.; Das Adhikari, S.; Pradhan, N. Tuning the Size of CsPbBr3 Nanocrystals: All at One Constant Temperature. *ACS Energy Letters* **2018**, *3*, 329−334.
(19) Imran, M.; Ijaz, P.; Baranov, D.; Goldoni, L.; Petralanda, U.; Akkerman, Q.; Abdelhady, A. L.; Prato, M.; Bianchini, P.; Infante, I.; Manna, L. Shape-Pure, Nearly Monodispersed $CsPbBr_3$ Nanocubes Prepared Using Secondary Aliphatic Amines. *Nano Lett.* **2018**, *18*, 7822−7831.
(20) Hubbard, C. R.; Swanson, H. E.; Mauer, F. A. A silicon powder diffraction standard reference material. *J. Appl. Crystallogr.* **1975**, *8*, 45−48.
(21) Vovk, I. A.; Tepliakov, N. V.; Baimuratov, A. S.; Leonov, M. Y.; Baranov, A. V.; Fedorov, A. V.; Rukhlenko, I. D. Excitonic phenomena in perovskite quantum-dot supercrystals. *Phys. Chem. Chem. Phys.* **2018**, *20*, 25023−25030.
(22) Nestoklon, M. O.; Goupalov, S. V.; Dzhioev, R. I.; Ken, O. S.; Korenev, V. L.; Kusrayev, Y. G.; Sapega, V. F.; de Weerd, C.; Gomez, L.; Gregorkiewicz, T.; Lin, J.; Suenaga, K.; Fujiwara, Y.; Matyushkin, L. B.; Yassievich, I. N. Optical orientation and alignment of excitons in ensembles of inorganic perovskite nanocrystals. *Phys. Rev. B: Condens. Matter Mater. Phys.* **2018**, *97*, 235304.
(23) Cottingham, P.; Brutchey, R. L. On the crystal structure of colloidally prepared $CsPbBr_3$ quantum dots. *Chem. Commun.* **2016**, *52*, 5246−5249.
(24) Rodová, M.; Brožek, J.; Knížek, K.; Nitsch, K. Phase transitions in ternary caesium lead bromide. *J. Therm. Anal. Calorim.* **2003**, *71*, 667−673.
(25) Bowen, D. K.; Tanner, B. K. *High Resolution X-ray Diffractometry and Topography*; Taylor & Francis: London, 1998; p x, 252 p.
(26) Dhez, P.; Weisbuch, C.; North Atlantic Treaty Organization, Scientific Affairs Division. *Physics, Fabrication, and Applications of Multilayered Structures*; Plenum Press: New York, 1988; p xiii, 416 p.
(27) Schmidt, O. *Lateral Alignment of Epitaxial Quantum Dots*; Springer: Berlin, 2007; p xv, 707 p.
(28) Karle, I. L.; Karle, J. The Structure of the Tetrachloroethylene Molecule. *J. Chem. Phys.* **1952**, *20*, 63−65.
(29) Bein, B.; Hsing, H.-C.; Callori, S. J.; Sinsheimer, J.; Chinta, P. V.; Headrick, R. L.; Dawber, M. In situ X-ray diffraction and the evolution of polarization during the growth of ferroelectric superlattices. *Nat. Commun.* **2015**, *6*, 10136.

DOI: 10.1021/acsmaterialslett.9b00217
ACS Materials Lett. 2019, 1, 272−276